JACS
JOURNAL OF THE AMERICAN CHEMICAL SOCIETY
Article
pubs.acs.org/JACS

High-Magnesian Calcite Mesocrystals: A Coordination Chemistry Approach

Jos J. M. Lenders,[†] Archan Dey,[†] Paul H. H. Bomans,[†] Jan Spielmann,[‡] Marco M. R. M. Hendrix,[†] Gijsbertus de With,[†] Fiona C. Meldrum,[§] Sjoerd Harder,*[,∥] and Nico A. J. M. Sommerdijk*[,†]

[†]Laboratory of Materials and Interface Chemistry, Eindhoven University of Technology, P.O. Box 513, 5600 MB Eindhoven, The Netherlands

[‡]Fakultät für Chemie, Universität Duisburg-Essen, Universitätsstrasse 5, 45117 Essen, Germany

[§]School of Chemistry, University of Leeds, Woodhouse Lane, Leeds LS2 9JT, United Kingdom

[∥]Stratingh Institute for Chemistry, University of Groningen, Nijenborgh 4, 9747 AG Groningen, The Netherlands

Supporting Information

ABSTRACT: While biogenic calcites frequently contain appreciable levels of magnesium, the pathways leading to such high concentrations remain unclear. The production of high-magnesian calcites in vitro is highly challenging, because Mg-free aragonite, rather than calcite, is the favored product in the presence of strongly hydrated Mg^{2+} ions. While nature may overcome this problem by forming a Mg-rich amorphous precursor, which directly transforms to calcite without dissolution, high Mg^{2+}/Ca^{2+} ratios are required synthetically to precipitate high-magnesian calcite from solution. Indeed, it is difficult to synthesize amorphous calcium carbonate (ACC) containing high levels of Mg, and the Mg is typically not preserved in the calcite product as the transformation occurs via a dissolution−reprecipitation route. We here present a novel synthetic method, which employs a strategy based on biogenic systems, to generate high-magnesian calcite. Mg-containing ACC is produced in a nonaqueous environment by reacting a mixture of Ca and Mg coordination complexes with CO_2. Control over the Mg incorporation is simply obtained by the ratio of the starting materials. Subsequent crystallization at reduced water activities in an organic solvent/water mixture precludes dissolution and reprecipitation and yields high-magnesian calcite mesocrystals with Mg contents as high as 53 mol %. This is in direct contrast with the polycrystalline materials generally observed when magnesian calcite is formed synthetically. Our findings give insight into the possible mechanisms of formation of biogenic high-magnesian calcites and indicate that precise control over the water activity may be a key element.

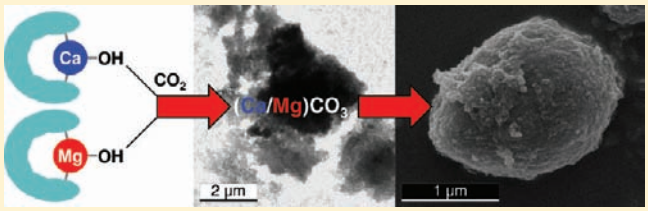

INTRODUCTION

Calcium carbonate is one of the most abundant and therefore important biominerals.[1] It represents the principal skeletal component of invertebrates, most of which are marine organisms, and therefore the biomineralization of this mineral makes a huge contribution to our ecological and geochemical systems. Biogenic calcites often contain significant concentrations of magnesium substituting for calcium in the crystal lattice.[2] Indeed, these Mg levels can frequently lie above 10 mol %, which categorizes the calcite as "high-magnesian calcite", and even levels as high as 45 mol % have been identified.[3] Further, organisms have developed strategies that can provide exceptional control over the level of Mg incorporation, as beautifully exemplified by sea urchin teeth, in which calcite plates and fibers containing 10−15% Mg are cemented together by a polycrystalline calcite matrix containing 40−45% Mg.[3]

As Mg^{2+} ions are strongly hydrated,[4] they poison the growth of calcite nuclei such that aragonite (which does not incorporate Mg) is preferentially precipitated rather than calcite if $[Mg^{2+}]:[Ca^{2+}] > 4:1$.[5] High-magnesian calcite is also more soluble and is hence thermodynamically less stable than aragonite. It is therefore highly challenging to produce high-magnesian calcite under mild solution conditions, and synthetic methods typically employ solid-state reactions at high temperatures and pressures[6] or solutions with high Mg^{2+}/Ca^{2+} ratios (up to 26:1).[7] In addition, while organisms can generate very large crystals of high-magnesian calcite, all synthetic equivalents have been proven resolutely polycrystalline.[8]

Investigation of the formation of calcium carbonate biominerals has shown that this often proceeds through an amorphous calcium carbonate (ACC) precursor phase.[9] In many cases, the ACC is stabilized by the incorporation of Mg^{2+} ions, possibly because they retard the loss of included water, which is necessary for crystallization.[10] Hence, high-magnesian calcite is certainly often preceded by high-magnesian ACC in vivo. Its conversion appears to occur via a solid-state transformation rather than full dissolution and reprecipitation[9] to maintain the incorporated Mg^{2+} in the product calcite phase.

Received: November 16, 2011
Published: December 14, 2011

   dx.doi.org/10.1021/ja210791p | J. Am. Chem.Soc. 2012, 134, 1367−1373

Attempts to generate high-magnesian calcite by mimicking this scenario synthetically are met by a number of problems: high-magnesian ACC can only be produced from solutions with high Mg^{2+}/Ca^{2+} ratios, and the Mg content of the precursor ACC phase is typically not translated into the product calcite lattice. The formation of ACC containing high Mg levels can be promoted using organic additives,[11] which can also enhance the Mg levels in calcite.[12] However, little control is generally achieved over the Mg content or the resulting polymorphs as the Mg^{2+} ions are released from the amorphous phase during its dissolution and reprecipitation, which commonly leads to the precipitation of polymorphic mixtures of aragonite, hydrated $MgCO_3$, and magnesian calcite.[13] That the strong Mg^{2+} hydration is key to this process is shown in the formation of magnesian calcites in water/alcohol mixtures, as reducing Mg^{2+} hydration by adding alcoholic cosolvents enhances the Mg incorporation in calcite.[14]

In this work, we report a novel method that leads to the formation of high-magnesian calcites. The strategy developed does not aim to copy nature, but instead takes its inspiration from the key processes that appear to lead to high-magnesian calcites. We have therefore employed conditions that first generate ACC including high Mg concentrations, and then quantitatively preserve these Mg levels in the resulting calcites. This strategy precludes crystallization of the ACC via a dissolution and reprecipitation route and enables us to investigate the role of bulk water in determining the product of Mg–ACC crystallization. Our method successfully produces high-magnesian calcite crystals with Mg levels up to 53 mol %.

RESULTS AND DISCUSSION

High-magnesian ACC was formed using a nonaqueous method, and it was then transformed into high-magnesian calcite by controlling the activity of the water in mixtures with tetrahydrofuran (THF) or dioxane (Scheme 1). The ACC

Scheme 1. Synthesis of High-Magnesian Calcite

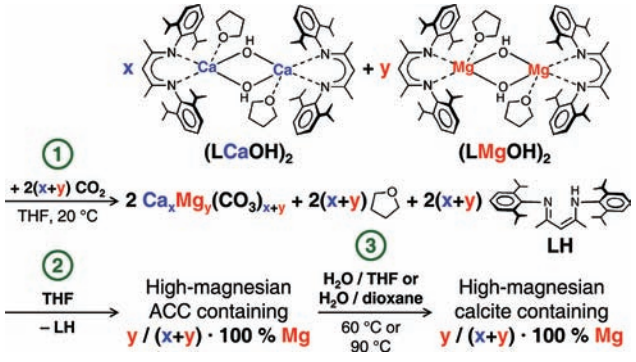

was synthesized starting from the coordination complexes $[(CH\{(CMe)(2,6\text{-}^{i}Pr_2C_6H_3N)\}_2)Ca(OH)\cdot THF]_2$, denoted as $(\mathbf{LCaOH})_2$, and its Mg analogue $(\mathbf{LMgOH})_2$ as the Ca and Mg precursors, respectively. ACC containing Ca ions only was synthesized by exposing $(\mathbf{LCaOH})_2$ in THF to CO_2, and a gel was produced alongside the protonated ligand (**LH**) (Scheme 1, step 1).[15] After the sample was washed with THF to remove the **LH** (Scheme 1, step 2), transmission electron microscopy (TEM) revealed that the product material consisted of 10–15 nm nanoparticles (Figure S1a,b). Selected-area electron diffraction (SAED) (Figure S1c) and powder X-ray diffraction (XRD) (inset in Figure S1c) confirmed that this material was amorphous and that it displayed two broad bands characteristic of ACC.[16] Energy-dispersive X-ray (EDX) spectroscopy demonstrated the presence of calcium (Figure S1d), thereby confirming the production of ACC. The ACC samples were also characterized using thermogravimetric analysis (TGA). Analysis of the pure Ca–ACC showed a major weight loss around 700 °C, corresponding to decomposition of $CaCO_3$ in CaO and CO_2 (Figure 1a).

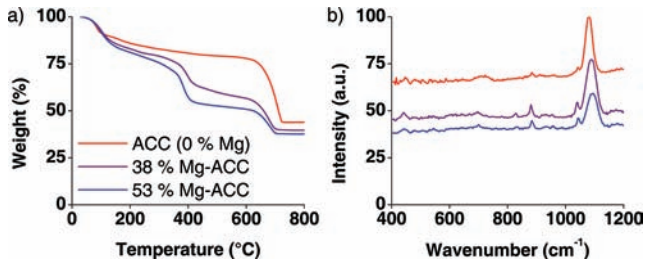

Figure 1. Characterization of the ACC, 38% Mg–ACC, and 53% Mg–ACC precursors by thermogravimetric analysis (a) and Raman spectroscopy (b). (a) As $MgCO_3$ decomposes around 400 °C, while $CaCO_3$ decomposes around 700 °C, the ratios between the two subsequent CO_2 losses in TGA reflected the quantitative Mg incorporation. (b) The broad carbonate peak at 1080 cm^{-1} typical for ACC broadened and shifted to 1090 cm^{-1} for 38% Mg–ACC and to 1092 cm^{-1} for 53% Mg–ACC, again demonstrating the incorporation of magnesium.

The possibility of preparing mixed Ca/Mg–ACC samples was then investigated by repeating these experiments with 60:40 and 50:50 molar mixtures of $(\mathbf{LCaOH})_2$ and $(\mathbf{LMgOH})_2$. This resulted in particles with sizes and morphologies similar to those of the pure Ca–ACC (Figures 2a,b and S2a,b). Diffraction

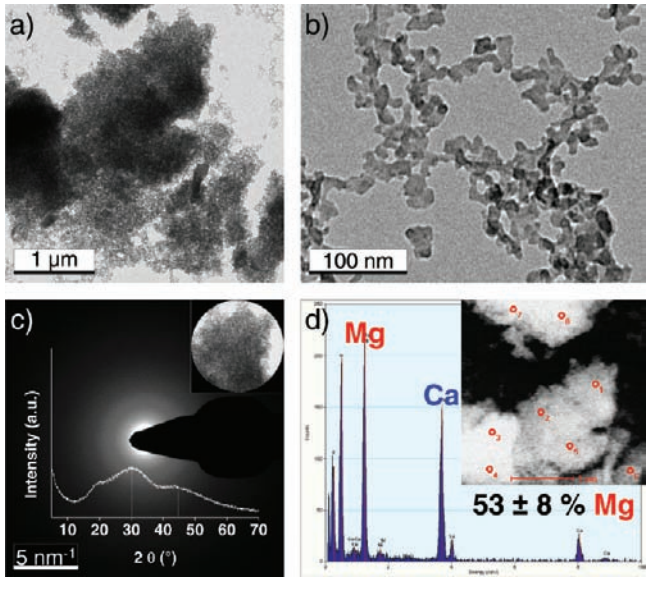

Figure 2. Characterization of the 53% Mg–ACC precursor. (a) Low-magnification TEM. (b) High-magnification TEM. (c) SAED pattern, insets show the selected area and the powder XRD pattern. (d) EDX, inset shows a scanning transmission electron microscopy (STEM) image (scale bar: 1 μm) with the measurement positions (8 out of 16) indicated.

techniques again showed that these materials were amorphous (Figures 2c and S2c), and EDX spectroscopy demonstrated Mg

dx.doi.org/10.1021/ja210791p | J. Am. Chem.Soc. 2012, 134, 1367–1373

Table 1. Properties of the Calcite Products Obtained after Crystallizing ACC Precursors

Mg content ACC (from EDX)	crystallization solvent (v/v)	crystallization temperature (°C)	calcite content (from XRD)	Mg content calcite (from EDX)	position (104) reflection (from XRD)	angular spread (104) reflection (from SAED)
0%	water	20	100%	0%	2θ = 29.5°	<1°
0%	10/90 water/THF	20	64%	0%	2θ = 29.5°	<1°
38 ± 5%	water	20	52%	21% (from XRD)	2θ = 30.0°	not determined
38 ± 5%	10/90 water/THF	60	100%	38 ± 3%	2θ = 30.8°	34°
38 ± 5%	5/95 water/THF	60	78%	35 ± 3%	2θ = 30.7°	16°
53 ± 8%	10/90 water/THF	60	76%	50 ± 4%	2θ = 31.1°	48°
53 ± 8%	5/95 water/THF	60	55%	46 ± 4%	2θ = 31.0°	40°
53 ± 8%	5/95 water/dioxane	90	44%	53 ± 5%	2θ = 31.1°	12°

contents of 38 ± 5 and 53 ± 8 mol % Mg for the 60:40 and 50:50 molar mixtures, respectively (Figures 2d and S2d). TGA analysis of the Mg–ACC samples showed an additional weight loss around 400 °C, corresponding to decomposition of $MgCO_3$ in MgO and CO_2 (Figure 1a). The $MgCO_3$ decomposition was accompanied by crystallization of the Mg–ACC into mixtures of calcite, vaterite, and periclase (MgO) (powder XRD not shown), similar to earlier thermal behavior studies.[17] The ratios between both CO_2 losses were well in agreement with the expected compositions, thereby confirming the almost perfect quantitative incorporation of the magnesium into the ACC.

All of the ACC samples also comprised ∼20% organics, which was primarily attributed to coordinated THF. Raman spectroscopy revealed that the carbonate peak at 1080 cm^{-1} for pure ACC had shifted to 1090 cm^{-1} for 38% Mg–ACC and to 1092 cm^{-1} for 53% Mg–ACC (Figure 1b), further demonstrating the Mg incorporation.[18] A peak broadening was also observed, which is attributed to the introduction of additional disorder in the ACC by the included Mg^{2+} ions.

Having demonstrated that this coordination chemistry route can lead to the formation of high-magnesian ACC, its use as a precursor to high-magnesian calcite was investigated under conditions of controlled water activity. Exposure of the pure Ca–ACC precursor to water at 20 °C resulted in conversion to micrometer-sized rhombohedral calcite crystals (Figure S3a,b). In contrast, the 38% Mg–ACC precursor crystallized to give a mixture of magnesian calcite (52%), aragonite (19%), and hydromagnesite ($Mg_5(CO_3)_4(OH)_2{\cdot}4H_2O$) (29%) under the same conditions (the concentrations of the different polymorphs were determined from the powder XRD pattern in Figure S4a). The Mg incorporation in the magnesian calcite was calculated to be 21% from the positions of the XRD reflections. This implies that during crystallization in water, a significant fraction of the magnesium is lost from the 38% Mg–ACC precursor and that it subsequently precipitates as hydromagnesite.

To reduce the likelihood of Mg^{2+} loss from the Mg–ACC during crystallization, crystallization was carried out at lower water activities in different water/solvent mixtures (Scheme 1, step 3), that is, in water/THF (5/95 or 10/90, v/v) or water/dioxane mixtures (5/95, v/v), and at different temperatures (20, 60, and 90 °C). The pure Ca–ACC precursor still readily crystallized in water/THF (10/90, v/v) at 20 °C, but now yielded a mixture of calcite (64%) and vaterite (36%) rather than pure calcite (Figure S3c,d and Table 1). In contrast, the 38% Mg–ACC precursor remained amorphous in water/THF mixtures at room temperature (not shown), showing that the incorporation of Mg^{2+} dramatically stabilizes ACC. Repetition of this experiment at 60 °C did, however, result in crystallization, and a mixture of high-magnesian calcite (78%) and aragonite (22%) was produced in water/THF (5/95, v/v) (Figure S4b). TEM and scanning electron microscopy (SEM) revealed that the high-magnesian calcite crystals possessed uniform, elongated, almond-like morphologies and that they had sizes of ∼2 μm (Figure 3a,c). The SAED patterns of these crystals showed narrow diffraction bands with an angular spread of only 16° (Figure 3b). Significantly, EDX analysis of 12 randomly chosen high-magnesian calcite crystals showed a Mg content of 35 ± 3% (Figure 3d). This was also confirmed by the observed shift of the XRD reflections to larger angles with respect to pure calcite (Figure S4b and Table 1). Because Mg-free aragonite was also formed in this reaction, we speculate that some magnesium must have been lost during the crystallization and washing of the product. These experiments clearly show that quantitative translation of the Mg content of the ACC precursor into the calcite product can be achieved on control of the water activity.

The influence of the water activity on the crystallization process was therefore investigated in more detail. Increase in the water activity from α = 0.16 (water/THF, 5/95, v/v, 60 °C) to α = 0.33 (water/THF, 10/90, v/v, 60 °C)[19] led to the formation of nearly pure high-magnesian calcite, as shown by the almost exclusive appearance of high-magnesian calcite reflections in the powder XRD pattern (Figure S4c). We ascribe this result to faster crystallization kinetics, where the kinetic polymorph (high-magnesian calcite) is favored over the thermodynamic polymorph (aragonite). SEM and TEM again revealed an elongated crystal morphology (Figures 4a and S5a,b), but SAED pointed at an angular misorientation of 34° (Figure 4b), indicating that the crystal domains were not perfectly aligned. This observation may result from the faster crystallization kinetics. The Mg content was found to be 38 ± 3% by EDX (Figure S5d–f) and from the positions of the XRD reflections (Figure S4c and Table 1), which again confirmed quantitative Mg incorporation in the high-magnesian calcite.

Remarkably, quantitative retention of Mg^{2+} during the ACC–calcite transformation was even observed for the crystallization of the 53% Mg–ACC precursor in water/THF (10/90, v/v, 60 °C). Some aragonite (24%) was also formed in this reaction (Table 1). It is suggested that this is due to a higher stability of 53% Mg–ACC as compared to 38% Mg–ACC, which would lead to 53% Mg–ACC crystallizing more slowly, and aragonite formation is observed as a side reaction. Indeed, by reducing the water activity from α = 0.33 (water/THF, 10/90, v/v, 60 °C)[19] to α = 0.16 (water/THF, 5/95, v/v, 60 °C)[19] and then to α = 0.12 (water/dioxane, 5/95, v/v, 90 °C),[20] the amounts of high-magnesian calcite decreased from 76% to 55% to 44%, respectively, in favor of aragonite formation (Table 1). Importantly, however, TEM and SAED showed that the slower crystallization kinetics in water/dioxane also led to a higher degree of perfection of the crystals (Figure 5a,b).

dx.doi.org/10.1021/ja210791p | J. Am. Chem.Soc. 2012, 134, 1367–1373

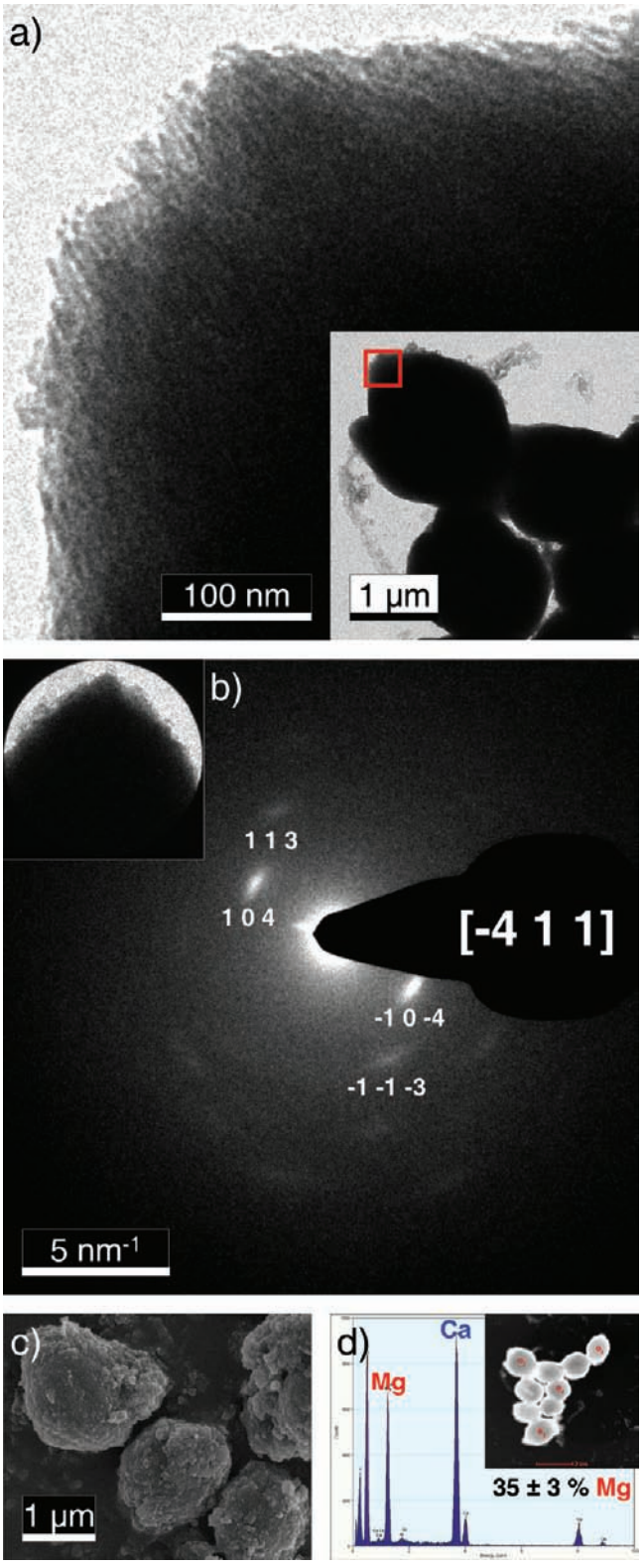

Figure 3. Characterization of the high-magnesian calcite crystals formed from 38% Mg–ACC in water/THF (5/95, v/v) at 60 °C. (a) TEM, inset shows a low-magnification with the area of the high-magnification TEM image indicated. (b) SAED pattern with indexation as high-magnesian calcite; inset shows the selected crystal. (c) SEM. (d) EDX, inset shows a STEM image with measurement positions indicated.

Narrow diffraction bands with an angular spread of only 12° were observed in SAED, while in water/THF mixtures the

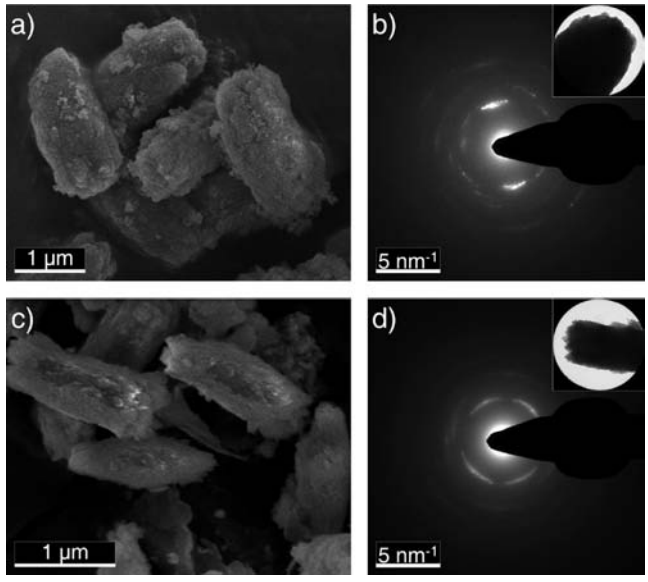

Figure 4. Characterization of the high-magnesian calcite crystals formed from 38% Mg–ACC (a,b) and 53% Mg–ACC (c,d) in water/THF (10/90, v/v) at 60 °C. (a,c) SEM and (b,d) SAED patterns showing the angular misorientations of the crystal domains (34° and 48°, respectively); insets show the selected crystals.

elongated crystals were found to have rather high mosaicity (Figure 4c,d) corresponding to angular misorientations up to 48° (Figure S6c and Table 1).

The spatial distribution of Ca and Mg inside the high-magnesian calcite crystals was also investigated by acquiring EDX line scans along the crystals. This revealed that the Ca and Mg profiles in all cases had similar shapes, which demonstrates that the magnesium is indeed equally distributed throughout the crystals, and is not expelled to the surface during Mg–ACC crystallization (Figures 5c,d, S5d–f, and S6d–f).

■ CONCLUSIONS

In our synthetic system, synthesis of high-magnesian ACC was achieved by performing the reaction under anhydrous conditions, and the nature of its transformation product was determined by the activity of the water in the solvent present. When pure water was used, dissolution of the Mg–ACC ions yielded magnesian calcite with a lower Mg content (Figure 6a), along with significant fractions of aragonite and hydromagnesite. In contrast, the Mg content of the Mg–ACC was conserved successfully in its daughter high-magnesian calcite when the crystallization was carried out at reduced water activities (Figure 6b). These lower activities were achieved by using mixtures of water and THF or dioxane and prevented the dissolution of the Mg–ACC. Yet further reduction in the water activity changes the kinetics of the crystallization process such that aragonite, which is thermodynamically favored over high-magnesian calcite, became the majority product (Figure 6c).

The results presented above show that our approach enables the formation of high-magnesian calcite crystals with predetermined Mg levels up to 53% through the direct conversion of Mg–ACC. We would like to draw attention to the fact that, even though the high-magnesian calcite peaks in powder XRD are rather broad (Figure S4), which is indicative of small crystal domain sizes, a number of our high-magnesian calcite crystals show very little angular spread (Figures 3b and 5b and Table 1). This demonstrates that the crystalline units

dx.doi.org/10.1021/ja210791p | J. Am. Chem.Soc. 2012, 134, 1367–1373

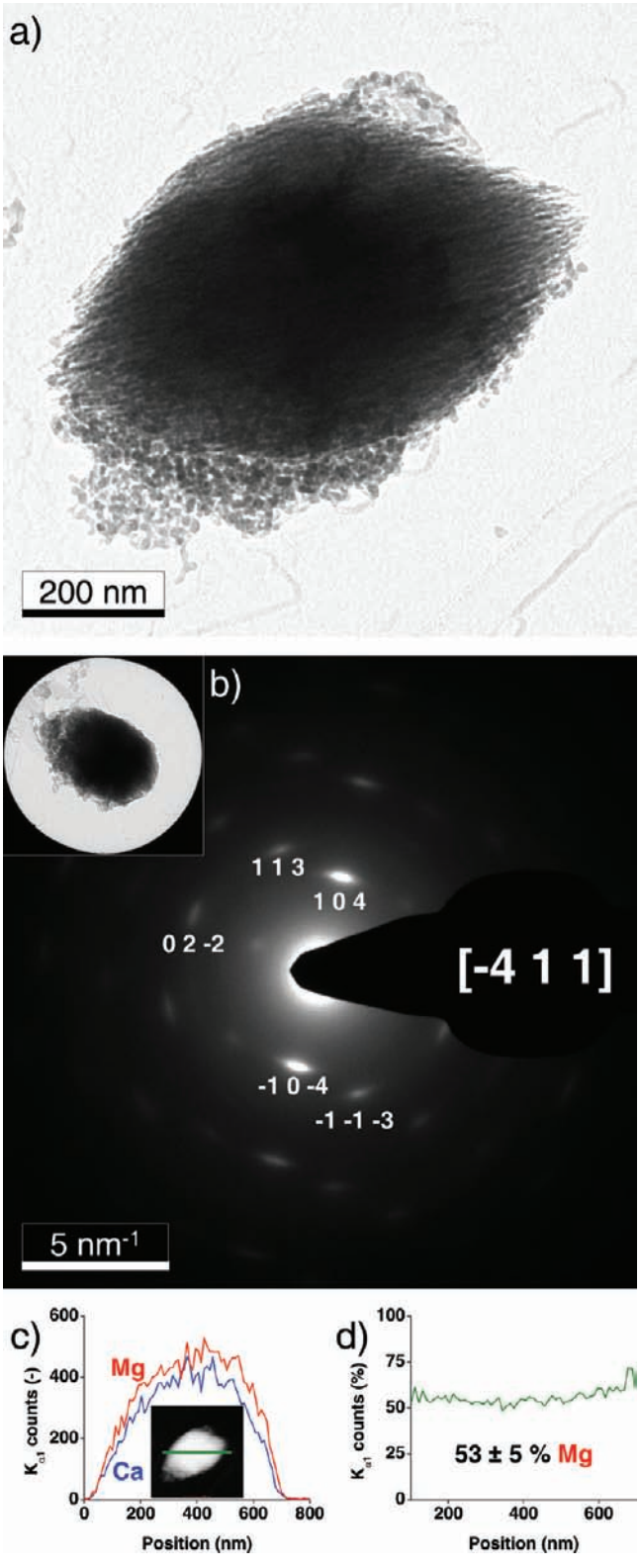

Figure 5. Characterization of the high-magnesian calcite crystals formed from 53% Mg–ACC in water/dioxane (5/95, v/v) at 90 °C. (a) TEM. (b) SAED pattern with indexation as high-magnesian calcite; inset shows the selected crystal. (c) Ca and Mg profiles exhibiting similar shapes; inset shows a STEM image of the crystal with the position of the EDX line scan indicated. (d) The Mg concentration is constant.

comprising the particles, which are apparent as a fibrous substructure visible by TEM at the perimeter of the particles

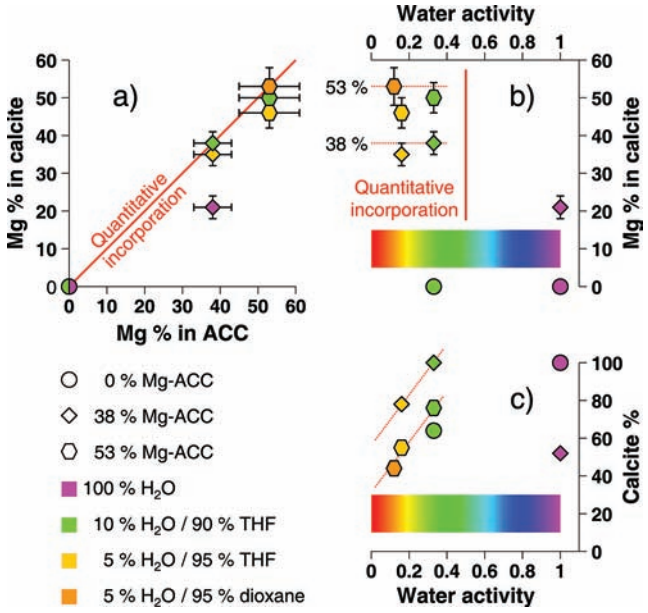

Figure 6. Summary of all results. (a) Mg content in the calcite product as a function of the Mg content in the ACC precursor, demonstrating quantitative incorporation in water/THF and water/dioxane mixtures. (b) Mg content in the calcite product as a function of water activity, demonstrating quantitative incorporation at reduced water activities. (c) Calcite content in the product as a function of water activity, demonstrating more calcite formation at intermediate water activities.

(Figures 3a and 5a), are well-aligned. These fibers also appear to be aligned along the elongation direction of the almond-like crystals. Such a structure is consistent with the idea of a "mesocrystal", which is strictly defined as a crystal exhibiting structure on the mesoscale.[21] Most commonly, it is used to describe a crystal that diffracts as a single crystal and is composed of mutually oriented nanoparticle units.[22] It has also been suggested that some calcite biominerals are mesocrystals,[23] and that they form via the crystallization of an ACC phase, leaving a memory of the original ACC particles in the calcite product.

The finding that we can produce high-magnesian calcite crystals with very little angular spread may also have significance to the question of how nature produces large single crystals of high-magnesian calcite. It is clear that direct precipitation of magnesian calcite from solution is highly challenging as the Mg^{2+} ions effectively poison the growth of the calcite nuclei. Subsequent growth of calcite crystals then most rapidly occurs on aggregation of these calcite nanoparticles, which leads to the polycrystalline high-magnesian calcite crystals observed experimentally. In contrast, organisms demonstrate that it is quite possible to produce large single crystals of high-magnesian calcite in aqueous environments. That they may actually be mesocrystals would provide one possible answer to how this is achieved. Examination of the strategies used in biology to create these minerals suggests there are at least two crucial steps: (1) the production of high-magnesian ACC and (2) the conversion of this precursor into high-magnesian calcite with retention of the included Mg^{2+} ions. Concerted crystallization of an aggregate of Mg–ACC particles could occur via a bridging mechanism, leading to a "single crystal" type product (as proposed in Figure 7). Further, that the original ACC particles are of nanometer dimensions circumvents the problem of the inhibited growth of the individual high-magnesian calcite crystallites by Mg^{2+}.

dx.doi.org/10.1021/ja210791p | J. Am. Chem.Soc. 2012, 134, 1367–1373

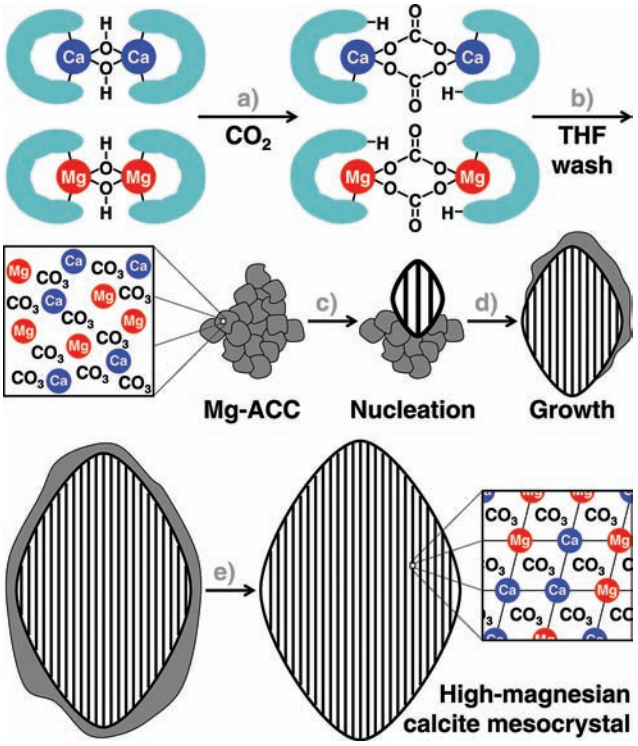

Figure 7. Proposed mechanism for the formation of high-magnesian calcite mesocrystals. (a) Reaction of a mixture of $(\mathbf{LCaOH})_2$ and $(\mathbf{LMgOH})_2$ with CO_2 leads to the formation of a gel built up by $(CaCO_3)_2$ and $(MgCO_3)_2$ units and the protonated ligand **LH**. (b) Removal of **LH** by washing with THF breaks the gel, resulting in the precipitation of aggregated high-magnesian ACC nanoparticles (the inset visualizes the amorphous nature of the material). (c) Nucleation of high-magnesian calcite occurs at reduced water activities by local reorganization of the Mg–ACC, thereby preserving the Mg/Ca incorporation. (d) Growth occurs subsequently by continuous deposition of Mg–ACC onto the crystal surface and co-oriented crystallization into a fibrous substructure (indicated by the stripe pattern). (e) Crystalline/amorphous core/shell intermediates (as demonstrated in Figure S7) precede the final high-magnesian calcite mesocrystals (the inset visualizes the crystalline nature of the material and the random Mg/Ca incorporation in the crystal lattice).

Many investigations on the crystallization of high-magnesian ACC in solution have been carried out, and all have yielded polycrystalline products.[8,11−14] Our experiments suggest that the key to producing high-magnesian calcite mesocrystals may be control over the water activity. This could be achieved biologically by transformation of ACC to calcite in an enclosed environment, isolated from the bulk solution,[24] as is observed, for example, on the formation of sea urchin larvae calcite single crystal spicules.[9a]

Although the reactions performed in this work, where organic solvents are used rather than aqueous media, may seem at first sight rather far removed from the usual biomimetic approaches to mineral formation, they may provide some possible answers to how nature may orchestrate the physiochemical constraints required for the formation of high-magnesian calcite and in particular single crystals of this phase. Indeed, to the best of our knowledge, this is the first time that calcite mesocrystals with such high Mg levels have been produced in a synthetic system. We anticipate that the method demonstrated here can be used to understand in more detail the role of water and water activity in the formation of high-magnesian calcite. Moreover, we believe that this approach will eventually allow us to design systems based on more benign media and additives, and that this will lead to the development of true biomimetic syntheses of materials beyond the high-magnesian calcite presented here.

■ ASSOCIATED CONTENT

Supporting Information

Materials and methods, characterization of the ACC and 38% Mg–ACC precursors, characterization of the crystals formed from ACC in water and water/THF (10/90, v/v) at 20 °C, powder XRD of the products obtained after crystallizing 38% Mg–ACC, and characterization of the high-magnesian calcite crystals formed from 38% Mg–ACC and 53% Mg–ACC in water/THF (10/90, v/v) at 60 °C. This material is available free of charge via the Internet at http://pubs.acs.org.

■ AUTHOR INFORMATION

Corresponding Author

n.sommerdijk@tue.nl; s.harder@rug.nl

■ ACKNOWLEDGMENTS

The research of N.A.J.M.S. is supported by a VICI grant of The Netherlands Organization for Scientific Research (NWO). We would like to acknowledge Fabio Nudelman and Maria Eriksson for their help with SEM and TGA, respectively.

■ REFERENCES

(1) Sommerdijk, N. A. J. M.; de With, G. *Chem. Rev.* **2008**, *108*, 4499–4550.

(2) (a) Clarke, F. W.; Wheeler, W. C. *The Inorganic Constituents of Marine Invertebrates*, 2nd ed.; U.S. Government Printing Office: Washington, 1922. (b) Vinogradov, A. P. *The Elementary Chemical Composition of Marine Organisms, Memoir II*; Sears Foundation for Marine Research: New Haven, 1953.

(3) (a) Schroeder, J. H.; Dwornik, E. J.; Papike, J. J. *Bull. Geol. Soc. Am.* **1969**, *80*, 1613–1616. (b) Ma, Y. R.; Cohen, S.; Addadi, L.; Weiner, S. *Adv. Mater.* **2008**, *20*, 1555–1559.

(4) Noyes, R. M. *J. Am. Chem. Soc.* **1962**, *84*, 513–522.

(5) (a) Kitano, Y. *Bull. Chem. Soc. Jpn.* **1962**, *35*, 1973–1980. (b) Simkiss, K. *Nature* **1964**, *201*, 492–493. (c) Berner, R. A. *Geochim. Cosmochim. Acta* **1975**, *39*, 489–504.

(6) (a) Graf, D. L.; Goldsmith, J. R. *J. Geol.* **1956**, *64*, 173–186. (b) Medlin, W. L. *Am. Mineral.* **1959**, *44*, 979–986.

(7) Glover, E. D.; Sippel, R. F. *Geochim. Cosmochim. Acta* **1967**, *31*, 603–613.

(8) (a) Cheng, X. G.; Varona, P. L.; Olszta, M. J.; Gower, L. B. *J. Cryst. Growth* **2007**, *307*, 395–404. (b) Jiang, J.; Gao, M. R.; Qiu, Y. H.; Wang, G. S.; Liu, L.; Cai, G. B.; Yu, S. H. *CrystEngComm* **2011**, *13*, 952–956.

(9) (a) Beniash, E.; Aizenberg, J.; Addadi, L.; Weiner, S. *Proc. R. Soc. London, Ser. B* **1997**, *264*, 461–465. (b) Politi, Y.; Arad, T.; Klein, E.; Weiner, S.; Addadi, L. *Science* **2004**, *306*, 1161–1164.

(10) (a) Addadi, L.; Raz, S.; Weiner, S. *Adv. Mater.* **2003**, *15*, 959–970. (b) Politi, Y.; Batchelor, D. R.; Zaslansky, P.; Chmelka, B. F.; Weaver, J. C.; Sagi, I.; Weiner, S.; Addadi, L. *Chem. Mater.* **2010**, *22*, 161–166.

(11) (a) Raz, S.; Weiner, S.; Addadi, L. *Adv. Mater.* **2000**, *12*, 38–42. (b) Wang, D. B.; Wallace, A. F.; De Yoreo, J. J.; Dove, P. M. *Proc. Natl. Acad. Sci. U.S.A.* **2009**, *106*, 21511–21516. (c) Long, X.; Ma, Y.; Qi, L. *Cryst. Growth Des.* **2011**, *11*, 2866–2873.

(12) (a) Wada, N.; Yamashita, K.; Umegaki, T. *J. Colloid Interface Sci.* **1999**, *212*, 357–364. (b) Stephenson, A. E.; DeYoreo, J. J.; Wu, L.; Wu, K. J.; Hoyer, J.; Dove, P. M. *Science* **2008**, *322*, 724–727. (c) Falini, G.; Fermani, S.; Tosi, G.; Dinelli, E. *Cryst. Growth Des.* **2009**, *9*, 2065–2072.

(13) Loste, E.; Wilson, R. M.; Seshadri, R.; Meldrum, F. C. *J. Cryst. Growth* **2003**, *254*, 206−218.
(14) Falini, G.; Gazzano, M.; Ripamonti, A. *Chem. Commun.* **1996**, *9*, 1037−1038.
(15) Ruspic, C.; Nembenna, S.; Hofmeister, A.; Magull, J.; Harder, S.; Roesky, H. W. *J. Am. Chem. Soc.* **2006**, *128*, 15000−15004.
(16) Faatz, M.; Grohn, F.; Wegner, G. *Adv. Mater.* **2004**, *16*, 996−1000.
(17) Kimura, T.; Koga, N. *Cryst. Growth Des.* **2011**, *11*, 3877−3884.
(18) Edwards, H. G. M.; Villar, S. E. J.; Jehlicka, J.; Munshi, T. *Spectrochim. Acta, Part A* **2005**, *61*, 2273−2280.
(19) Pinder, K. L. *J. Chem. Eng. Data* **1973**, *18*, 275−277.
(20) Goates, J. R.; Sullivan, R. J. *J. Phys. Chem.* **1958**, *62*, 188−190.
(21) Cölfen, H.; Antonietti, M. *Mesocrystals and Nonclassical Crystallization*; John Wiley & Sons: New York, 2008.
(22) Song, R. Q.; Cölfen, H. *Adv. Mater.* **2010**, *22*, 1301−1330.
(23) (a) Oaki, Y.; Imai, H. *Small* **2006**, *2*, 66−70. (b) Oaki, Y.; Kotachi, A.; Miura, T.; Imai, H. *Adv. Funct. Mater.* **2006**, *16*, 1633−1639. (c) Sethmann, I.; Worheide, G. *Micron* **2008**, *39*, 209−228.
(24) (a) Loste, E.; Park, R. J.; Warren, J.; Meldrum, F. C. *Adv. Funct. Mater.* **2004**, *14*, 1211−1220. (b) Stephens, C. J.; Ladden, S. F.; Meldrum, F. C.; Christenson, H. K. *Adv. Funct. Mater.* **2010**, *20*, 2108−2115. (c) Kim, Y.-Y.; Hetherington, N. B. J.; Noel, E. H.; Kröger, R.; Charnock, J. M.; Christenson, H. K.; Meldrum, F. C. *Angew. Chem. Int. Ed.* **2011**, *50*, 12572−12577.